

High-lying Rydberg atoms surviving intense laser fieldsMeng Zhao,^{1,2} YanLan Wang,^{2,3} Wei Quan ,^{2,3,*} XuanYang Lai,^{2,3} HongPing Liu ,^{2,3} JianDuo Lu,^{1,†} and XiaoJun Liu^{2,3}¹*Hubei Province Key Laboratory of Systems Science in Metallurgical Process, Wuhan University of Science and Technology, Wuhan 430081, China*²*State Key Laboratory of Magnetic Resonance and Atomic and Molecular Physics, Wuhan Institute of Physics and Mathematics, Innovation Academy for Precision Measurement Science and Technology, Chinese Academy of Sciences, Wuhan 430071, China*³*University of Chinese Academy of Sciences, Beijing 100049, China*

(Received 9 May 2021; revised 6 October 2021; accepted 11 October 2021; published 28 October 2021)

In this work, we have experimentally and theoretically investigated the high-lying Rydberg state excitation for noble gas atoms subject to an intense near-infrared laser field. To obtain the signal of these high-lying Rydberg atoms which are further ionized by a constant electric field (F_c), coincident detection of the photoelectrons and photoions with well-chosen arrival times is performed. Based on a fitting to the time dependence of the coincidentally measured photofragment yields with a semiempirical formula, we can extract a principal quantum number distribution (PQND) of the population of the excited states in a range closely related to the strength of F_c . The extracted valid PQND is in qualitative agreement with a semiclassical model calculation. Our work thus provides a method to extract the PQND and study the ultrafast high-lying Rydberg state excitation.

DOI: [10.1103/PhysRevA.104.043115](https://doi.org/10.1103/PhysRevA.104.043115)**I. INTRODUCTION**

The ionization of atoms and molecules subject to intense laser fields induces a variety of highly nonlinear phenomena, such as high-order above-threshold ionization (HATI) [1], nonsequential double ionization (NSDI) [2], and high-order harmonic generation (HHG) [3]. In the limit of high intensity and long wavelength, these highly nonlinear phenomena can be described with a rescattering model [4,5]. In this model, the valence electron is first liberated through tunneling; then, the freed electron is accelerated by the laser field and, depending on the phase of the laser field when tunneling happens, it may return to the ionic core; finally, the electron may elastically scatter on the core (HATI), or kick out another electron from the core (NSDI), or recombine with the core to emit a high-energy photon simultaneously (HHG). The physical picture revealed by this model is widely accepted and many interesting strong-field phenomena can be well explained by this model.

Recently, a phenomenon of Rydberg state excitation (RSE) has been experimentally investigated and comprehended with a mechanism of frustrated tunneling ionization (FTI) [6], which is physically compatible with the rescattering model. Based on FTI, if the freed electron does not gain enough drift energy from the laser field, it could be captured by the Coulomb field of the residual parent core. Essentially, the FTI scenario replenishes the families of phenomena relevant to the rescattering model. Indeed, the mechanism of FTI has been widely applied to comprehend the numerical results (see, e.g., Refs. [7–10]) and can properly predict the main features of RSE, such as the laser polarization dependence of excitation

atom yields [6], the acceleration of neutral atoms [11,12], and the principal quantum number distribution (PQND) of the population of the excited states [6,13,14]. Moreover, the energetic excited neutral H* [15] and N* [16] fragments from the dissociation of the corresponding molecules in strong laser fields have been observed and explained with FTI and the ultrafast process of frustrated nonsequential double ionization has been numerically studied [17]. Multiply frustrated tunneling ionization-induced dissociation of the argon dimer induced by intense linearly polarized ultrashort laser fields has been observed [18].

In contrast, the experimental and numerical results with features beyond the predictions of FTI have also been documented. Distinct quantum features, such as the unprecedented [19] and periodic [20] enhancements of excitation yields, and the oscillation behavior of the ratio between the Rydberg atom yields for N₂ and Ar [21], have been shown in near-infrared experiments. Based on the numerical solution of the time-dependent Schrödinger equation (TDSE) [22,23], it is predicted that the yields of both excitation and ionization display strong modulations that are out of phase in relation to each other as a consequence of channel closing in multiphoton processes. To comprehend the modulations in the intensity dependence of RSE, a mechanism of coherent capture [24] has been proposed. Recently, these modulations have been experimentally observed and a clear transition of the underlying physical mechanism of strong-field atomic excitation from multiphoton resonance to coherent recapture has been demonstrated experimentally [25]. As discussed above, a comprehensive understanding of the physical origin of the RSE is still in progress.

Note that, with the experimental procedure employed by most of the documented works (see, e.g., Refs. [6,13,21]), only the excited atoms with principal quantum number of $n < 30$ have been measured and investigated. Compared to the

*charlywing@wipm.ac.cn

†lj316@163.com

Rydberg atoms with $n < 30$, the high-lying Rydberg atoms with $n \geq 100$ surviving the intense laser field have not been well studied. Thereby it is attractive to study higher-lying Rydberg atoms to fully comprehend the underlying physics of RSE. Only recently, Larimian *et al.* [26–28] presented a procedure of detection of high-lying Rydberg atoms and they successfully extracted the yields of the high-lying Rydberg atoms by coincidence measurements of the electron and ion emission from the atoms and molecules subject to strong laser fields. Zhang *et al.* extended this procedure to study frustrated double ionization of small molecules [29,30]. Still, more information, e.g., the PQND of the high-lying Rydberg atoms, which may provide more clues to the underlying mechanism of RSE in intense laser field, is not yet available. In fact, it is very difficult to extract directly in experiments the PQND of high-lying Rydberg atoms because their energy spacings are too small to be resolved.

In this work, we propose a procedure to extract the PQND of high-lying Rydberg atoms excited by an intense near-infrared laser field. The PQND, in a principal quantum number range closely related to the strength of the dc electric field (F_c) of the spectrometer, is obtained by fitting the measured time dependence of the dc-field-ionization yields of surviving Rydberg atoms with a semiempirical formula. This formula can give a featured decaying curve of the surviving population for each Rydberg state subject to a static electric field (see Sec. III for details). With increasing the strength of F_c , we can obtain the PQNDs at a series of principal quantum number ranges. The extracted PQNDs at different F_c are consistent with each other and qualitatively match the semiclassical calculations.

This paper is organized as follows. The experimental method is described in the following section. In Sec. III, the details of the procedure to extract the PQNDs of high-lying Rydberg atoms are given. The semiclassical model is briefly described in Sec. IV. In Sec. V, the experimental and numerical results are presented and discussed. Finally, a conclusion is given in Sec. VI. Atomic units (a.u.) are used throughout unless otherwise indicated.

II. EXPERIMENTAL METHOD

The experiments have been performed with a cold target recoil ion momentum spectroscopy (COLTRIMS) [31,32]. Laser pulses with a center wavelength of 800 nm, a repetition rate of 5 kHz, and a pulse duration of 30 fs are generated by a commercial Ti:sapphire femtosecond laser system (FEMTOPOWER compact PRO CE-Phase HP/HR). The single-pulse energy is up to 0.8 mJ and the output energy is controlled with a neutral density filter. A broadband thin-film polarizer is employed to ensure the linear polarization.

The laser beam is directed into the vacuum chamber of the COLTRIMS apparatus and focused by an on-axis spherical mirror ($f = 75$ mm) onto a cold supersonic atomic beam. With a constant and uniform dc electric field, the photoions and photoelectrons are extracted to the ion and electron position-sensitive microchannel plate (MCP) detectors with delay line anodes equipped, respectively. A constant and uniform magnetic field generated by a pair of Helmholtz coils is further applied to confine the photoelectron movement in

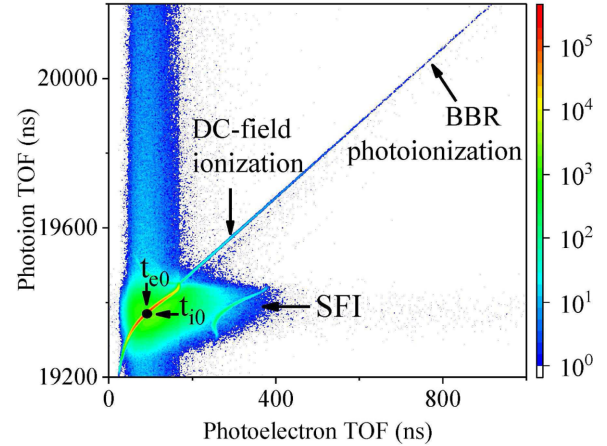


FIG. 1. PEPICO spectrum for Ar subject to a near-infrared multi-cycle laser field at 1.7×10^{14} W/cm² and a dc field with the strength of 2.2 V/cm. The pulse duration is 30 fs. BBR photoionization and SFI indicate the contributions from blackbody radiation photoionization and strong laser field ionization, respectively. “DC-field ionization” indicates the contributions from dc field ionization of the high-lying Rydberg states. See text for details.

the plane perpendicular to the dc electric field. The three-dimensional momenta of photoelectrons and photoions can be retrieved from their time of flight (TOF) and the impact positions on the corresponding detectors. Details on our COLTRIMS apparatus can be found in Refs. [33–36].

Note that the dc electric field, usually employed to extract the photoions and photoelectrons in COLTRIMS, plays a crucial role to measure the signal of the high-lying Rydberg atoms in this work. In fact, the dc electric field is still present after the atoms are excited by the ultrafast laser field. If the principal quantum number is high enough, the Rydberg atom can be ionized by the dc electric field. After that, the produced ion and electron will fly towards the corresponding detectors and hit them after further acceleration by the dc electric field. To obtain the signal of high-lying Rydberg atoms which are ionized by the dc electric field, coincident detection of the photoelectrons and photoions with well-chosen arrival times is performed. In Fig. 1, a typical photoelectron-photoion-coincidence (PEPICO) spectrum for Ar subject to an 800-nm laser field at 1.7×10^{14} W/cm² and a dc electric field with the strength of 2.2 V/cm is presented. As shown in this figure, the most prominent feature is the main peak at the electron TOF $t_e \sim 90$ ns (indicated with t_{e0}) and the ion TOF $t_{ion} \sim 19370$ ns (indicated with t_{i0}), which represents the outcome of the strong laser field ionization (SFI) for Ar, as discussed in Refs. [26,27].

The SFI main peak sets a time reference for the delayed emission of ions and electrons from dc electric field ionization of Rydberg atoms. t_{i0} and t_{e0} are the time spent by the ions and electrons with initial velocities of $v_{i,e} \approx 0$ to fly from the focus to their corresponding detectors. In contrast to the SFI, emission of ions and electrons from the dc electric field ionization of the Rydberg atoms could be delayed by Δt . The number of the measured ionized Rydberg atoms, $W(\Delta t)$, is proportional to the population of the Rydberg state surviving the strong laser field and dc electric field. Thus, the postpulse ionized

Rydberg states with a delay of Δt after the strong laser field excitation will locate at the coordinate of $(t_{e0} + \Delta t, t_{i0} + \Delta t)$ and the Δt dependence of $W(\Delta t)$ will give rise to a line parallel to the diagonal in Fig. 1.

Only the ions and electrons with well-chosen arrival times are employed to extract PQNDs. As shown in Ref. [26], for the dc field with the strength of several V/cm, the excited atoms significantly contributing to the dc field ionization yields usually possess the principal quantum number of $n \geq 100$ and the yields are significant for Δt in the temporal scale of hundreds of nanoseconds. Therefore, only the events with arrival times short enough to remove the influence of blackbody radiation (BBR) [26] and, in the meantime, long enough to avoid the influence of SFI contributions are studied in our work. In this paper, this temporal interval is termed the effective temporal interval (ETI). In experiment, the ETI should be well chosen to make sure that the yields are relatively high and can be safely attributed to dc electric field ionization of the Rydberg states produced by the strong laser fields. Apparently, the ETI is closely related to the strength of the dc electric field and the principal quantum number range of the Rydberg atoms contributing significantly in the ETI can be altered conveniently by varying the strength of the dc electric field. Note that, although it is in the range of the ETI where the dc electric field ionization yields can be measured and analyzed, the instant for PQND to be obtained in this work is right after the laser pulse ends.

III. THE PROCEDURE TO EXTRACT PQNDS OF HIGH-LYING RYDBERG ATOMS

In this work, a procedure has been developed to extract the PQND from the experimental data. With the data given in Fig. 1, the time dependence of the yields of postpulse ionized Rydberg states can be obtained [see Fig. 2(a)]. On the other hand, the time dependence of the survived population of each high-lying Rydberg state for a hydrogen atom subject to a dc electric field has already been well documented and an accurate semiempirical formula has been given (see, e.g., Ref. [37]). Considering the large distance between the ionic core and the valence electron for the high-lying Rydberg atom concerned in this work, it can be understood that the structure of the core can be safely ignored and the high-lying Rydberg state of any other atom resembles that of a hydrogen atom very much. Thus, we exploit the calculated time-delay distributions of H Rydberg states in a dc electric field to fit the measured time dependence of the yields of postpulse ionized Rydberg atoms and the contribution of the Rydberg state is proportional to the corresponding fitting coefficient. The details of this procedure are given below.

The width of a Stark level (i) of a Rydberg hydrogen atom subject to an electric field F_c can be given by a semiempirical formula [37],

$$\Gamma_i = \frac{(4R)^{2n_2+|m|+1}}{n^3 n_2! (n_2 + |m|)!} \exp \left[-\frac{2}{3}R - \frac{1}{4}n^3 F_c \left(34n_2^2 + 34n_2|m| + 46n_2 + 7m^2 + 23|m| + \frac{53}{3} \right) \right], \quad (1)$$

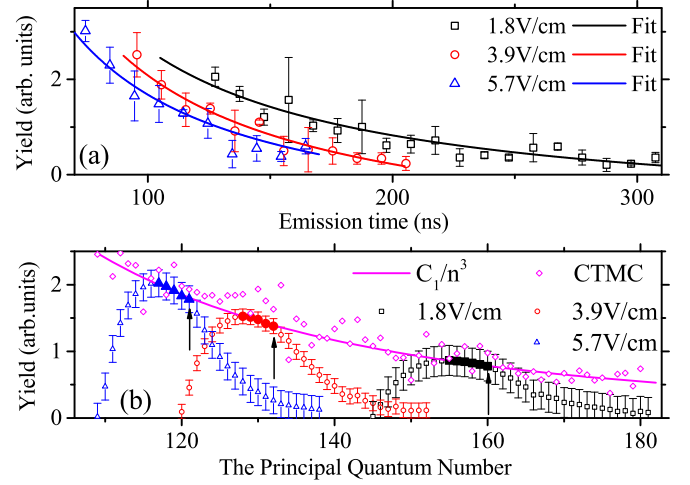


FIG. 2. (a) The measured time dependence of the yields of post-pulse ionized Rydberg states of Ar at a series of dc electric fields. The fitting results are depicted by solid curves. (b) The extracted PQNDs for the data presented in (a). The laser intensity is 1.9×10^{14} W/cm² and the wavelength is 800 nm. The black squares, red circles, and blue triangles indicate (a) the measured data and (b) the extracted PQND at 1.8, 3.9, and 5.7 V/cm, respectively. The magenta diamonds in (b) indicate the calculated PQND by the semiclassical model described in Sec. IV. See text for details.

where n is the principal quantum number, m the magnetic quantum number, and n_1 and n_2 the parabolic quantum numbers. n is related to n_1 , n_2 , and m through

$$n = n_1 + n_2 + m + 1. \quad (2)$$

Note that, in this work, $m = 0$ because of the transition selection rule in a linearly polarized laser field. The parameter R [37,38] can be achieved by

$$R = \frac{(-2E_i)^{3/2}}{F_c}, \quad (3)$$

where E_i is the Stark energy calculated by the fourth-order perturbation theory and can be expressed as [39]

$$E_i = -\frac{1}{2n^2} + \frac{3}{2}nqF_c + \frac{n^4}{16}(-17n^2 + 3q^2 + 9m^2 - 19)F_c^2 + \frac{3}{32}n^7q(23n^2 - q^2 + 11m^2 + 39)F_c^3 + \frac{n^{10}}{1024}(-5487n^4 - 147q^4 + 549m^4 - 1806n^2q^2 + 3402n^2m^2 + 1134m^2q^2 - 35182n^2 - 5754q^2 + 8622m^2 - 16211)F_c^4, \quad (4)$$

where

$$q = n_1 - n_2. \quad (5)$$

The time dependence of the population of the Stark level in a dc electric field can be described by

$$W_i(t) = N_i e^{(-\Gamma_i \times t)}, \quad (6)$$

where N_i is the number of atoms populated in the Stark level right after the laser pulse ends and Γ_i can be given by Eq. (1).

The time dependence of the total ionization rate in the Stark levels within one n manifold can be given by [40]

$$W_n(t) = \sum_i [\Gamma_i W_i(t)]. \quad (7)$$

As discussed in Sec. II, in experiments, only the ionization yields in the ETI are relevant in this work. According to Ref. [40] and discussions above, for any chosen strength of F_c , $W_n(t)$ will be significant in the ETI if the principal quantum number, n , locates in a specific range, which is closely related to the strength of F_c . For the Rydberg state with a principal quantum number smaller than the lower limit of the range, the ionization rate is too low to be detected. However, for the Rydberg state with a principal quantum number larger than the higher limit of the range, the ionization rate will be so large that the population survived in the ETI is negligible. Considering that the length of the range is finite, it is expected that, in the ETI, the measured time dependence of the dc-field-ionization rate of surviving Rydberg atoms can be fitted by a finite number of decaying curves described with Eq. (7), i.e.,

$$W(t) = \sum_n [a_n \times W_n(t)], \quad (8)$$

where a_n is the fit coefficient, which is proportional to the population of the corresponding Rydberg state with principal quantum number of n . Based on the fitting result of a_n , the PQND of RSE induced by the laser field can be further obtained. As discussed above, the PQND obtained with the above procedure is within a limited principal quantum number range which is closely related to the strength of F_c . To achieve the PQND in a larger principal quantum number range, it is necessary to increase or decrease the strength of F_c in experiment to alter the ETI.

IV. SEMICLASSICAL MODEL

The excitation dynamics are numerically simulated with a semiclassical model, which is shown to be invaluable and efficient in providing intuitive understanding and predictive power. As documented (see, e.g., Refs. [41–45]), this model has already been employed to study the strong-field ionization successfully. In particular, in the semiclassical calculations, the tunneled electrons, which are captured by the Coulomb potential after the laser pulse ends, can be identified conveniently.

In the semiclassical calculation, it is assumed that the electron is first released from a bound state to a continuum state through tunneling [46,47] and the following dynamics are described by a classical Newtonian equation [48–53]:

$$\frac{d^2 \vec{r}}{dt^2} = -\vec{F}(t) - \nabla V(r), \quad (9)$$

where $\vec{F}(t) = (0, 0, F_z(t))$ is the linearly polarized laser electric field with $F_z(t) = a(t)F_0 \cos(\omega t)$. Here, F_0 is the peak electric field strength, ω the laser angular frequency, and $a(t)$ the envelope function:

$$a(t) = \begin{cases} \cos^2\left(\frac{\omega t}{2N_c}\right), & -\frac{N_c}{2} \leq t \leq \frac{N_c}{2} \\ 0, & t < -\frac{N_c}{2}, t > \frac{N_c}{2} \end{cases}, \quad (10)$$

where N_c is the number of laser cycles. In this work, $N_c = 30$ corresponds to the pulse duration (full width at half maximum) of around 30 fs employed in the experiments. The effective potential exerted on the tunneled electron is given by

$$V = -\frac{Z_{\text{eff}}}{r}, \quad (11)$$

where Z_{eff} is the effective nuclear charge and r denotes the distance between the tunneled electron and the parent ionic core.

In this work, the laser polarization direction is along the z axis. The initial coordinates of the tunnel ionized electron are $x_0 = y_0 = 0$ and $z_0 = -\frac{1}{2}\eta_0$, where η_0 can be determined by solving the equation of $-(\frac{1}{4\eta} + \frac{1}{8\eta^2} + \frac{1}{8}E\eta) = -\frac{1}{4}I_p$ [48]. The tunneled electron is assumed to have a zero initial longitudinal velocity and a nonzero initial transverse velocity, v_{per} , which is given by a random value in the momentum range of (0, 1.00 a.u.). Here, θ is the angle between v_{per} and the x axis. Thus, the initial velocities are given by $v_{x0} = v_{\text{per}} \cos(\theta)$, $v_{y0} = v_{\text{per}} \sin(\theta)$, and $v_{z0} = 0$. The weight of each electron orbit is calculated by [47]

$$\begin{aligned} w(t_0, v_{\text{per}}) &= w(0)w(1), \\ w(0) &= \left| \frac{(2|I_p|)^2}{|F(t_0)|} \right|^{2/\sqrt{2|I_p|}-1} \exp \left[\frac{-2(2|I_p|)^{3/2}}{3|F(t_0)|} \right], \\ w(1) &= \frac{v_{\text{per}}\sqrt{2|I_p|}}{\pi|F(t_0)|} \exp \left[\frac{-v_{\text{per}}^2\sqrt{2|I_p|}}{|F(t_0)|} \right], \end{aligned} \quad (12)$$

where t_0 indicates the instant of tunneling.

To numerically identify the electron captured by the Coulomb potential, we search for the trajectories with the energies $E_{\text{sum}} < 0$ after the laser pulse ends. E_{sum} indicates the sum energy of kinetic energy and potential energy of the electron. Considering that the high-lying Rydberg atom resembles a hydrogen atom, we use the formula of the hydrogen energy level, $E = \frac{1}{2n^2}$, to obtain the principal quantum number, n , corresponding to E_{sum} . The weights of these trajectories are summed up to calculate the yields of the excitation [6]. Thus, the PQND can be achieved by the semiclassical model.

V. RESULTS AND DISCUSSION

In Fig. 2(a), the measured time dependence of the yields of postpulse ionized Rydberg states of Ar at the dc electric fields with the strengths in the range 1.8–5.7 V/cm are presented. Compared to the results in Ref. [26], the data here are presented in a shorter time-delay regime. Nevertheless, the main features of our measurements are consistent with the documented data, including that the yields drop rapidly with respect to time delay and the trend becomes more and more moderate with increasing time delay. As discussed in Sec. III, a series of Rydberg states contributes to the postpulse ionization yields at each time delay and the yields decrease due to the decay of the high-lying Rydberg states subject to the dc electric field. Here, we exploit the calculated time-delay distributions of H Rydberg states in a dc electric field to fit the measured time dependence of the yields of postpulse ionized Rydberg atoms and the results are shown by solid

curves in Fig. 2(a). The PQND can be obtained with the fitting coefficients.

The extracted PQNDs for Ar at 1.9×10^{14} W/cm² are shown in Fig. 2(b) with black squares, red circles, and blue triangles for the data at 1.8, 3.9, and 5.7 V/cm, respectively. It can be found that the PQND exhibits a hump structure. This result validates our assumption that the yields of a finite number of surviving Rydberg states will dominate in the ETI. The PQNDs which can be faithfully extracted from the measurements are termed as valid PQNDs in this work and indicated by solid symbols in Fig. 2(b). For the Rydberg state with principal quantum number lower than the lowest n of the valid PQND, with decreasing principal quantum number, the yield in the ETI decreases so fast that the extracted population starts to decline. On the other hand, for the Rydberg state with principal quantum number larger than the highest n of the valid PQND, the yield of the postpulse ionized Rydberg state drops fast because the ionization rates are relatively large and the surviving population before the ETI already becomes too small to contribute significantly to the measurement. Thus, a point of inflection of the PQND curve [see black vertical arrows in Fig. 2(b)] suddenly comes out right at the end of the solid symbols. The mechanism discussed above can be confirmed by the experimental investigations of the dc field strength dependence of PQNDs. As shown in Fig. 2(b), with decreasing strength of the dc electric field, the PQND shifts to the regime of larger principal quantum number. In the meantime, at each strength of dc electric field, the valid PQNDs can be easily identified by the PQND summit and also the point of inflection of the PQND curve.

To compare and verify the extracted PQNDs shown in Fig. 2(b), numerical calculations have been performed with the semiclassical model described in Sec. IV and the calculations are indicated with magenta diamonds in the same panel. It looks like a (magenta solid) curve of $\frac{C_1}{n^3}$, where C_1 is a constant, can well reproduce the calculated PQND. According to the semiclassical calculations (see, e.g., Ref. [54]), for the experimental parameters concerned in this work, the level energy dependence of the high-lying Rydberg state population is close to a horizontal line. On the other hand, the level spacings of the high-lying Rydberg states of H are approximately proportional to $\frac{1}{n^3}$. Therefore, we can understand that the PQND of a hydrogenlike atom will match approximately the prediction of $\frac{C_1}{n^3}$.

With a comparison of the extracted valid PQNDs (indicated by solid symbols) and the semiclassical calculations, a good agreement can be identified. Note that the focal averaging effect is not significant here because, according to the semiclassical calculations at a series of intensities, the PQND of the high-lying Rydberg states is not sensitive to the laser intensity in the range concerned in this work. The agreement between the extracted PQNDs and the calculations indicate that our method to extract the PQND is robust and reliable.

Note that our method can only be applied to high-lying Rydberg state excitation for noble gas atoms or simple molecules subject to an intense laser field. Because the field ionization model described in Sec. III is based on an assumption of a hydrogenic atom, there are two cases when the semiempirical formula is not accurate, i.e., the principal quantum number, n , is not large enough, e.g., $n \leq 5$, or the orbital angular momen-

tum quantum number, l , is dominated by $l = 0$. In these two cases, the influence of the atomic or molecular core cannot be ignored and the assumption of a hydrogenic atom may become unreasonable and the semiempirical formula may not be applied. In this work, the principal quantum number, n , is larger than 100, and, in the meantime, the Rydberg state excitation process in a strong field gives rise to a significant deviation of the orbital angular momentum quantum number from $l = 0$ (see, e.g., Ref. [22]). Thus, the electron probability distribution cannot penetrate the atomic core and the core structure can be safely ignored. Indeed, the dc electric field ionization of these high-lying Rydberg atoms is usually considered hydrogenic field ionization (see, e.g., Refs. [55,56]).

VI. CONCLUSION

In this work, we propose a method to extract the PQNDs of Rydberg states produced by strong laser field. It is demonstrated that, at each dc electric field, the extracted valid PQND of Ar shows a monotonically decreasing trend with rising principal quantum number and shifts to a regime of larger principal quantum number at lower strength of dc electric field. The extracted valid PQND can be qualitatively reproduced by a semiclassical model.

In the future, the procedure can be applied to experimentally investigate the excitation phenomena for atoms and molecules subject to an intense laser field, especially for the experiments with COLTRIMS. With the extracted PQND of the high-lying Rydberg state, more details of the ultrafast excitation process may be revealed from the elusive time-dependent information of excitation yields. Moreover, theoretical investigations of the PQND will be encouraged and the mechanism of RSE can be deeply explored.

On the other hand, the PQND of the high-lying Rydberg state might be relevant to many issues, which can be investigated experimentally with the procedure developed in this work. It could be interesting to explore PQNDs of high-lying Rydberg atoms produced with all kinds of tailored laser fields, such as polarization gating [57], bicircular fields [58], etc. Furthermore, the procedure may be extended to study the PQNDs of more complicated system, e.g., excited cations, which is paramount to comprehend the double-ionization process, and molecules (or molecular fragments). Considering that the excitation process is ubiquitous during the interaction of intense laser with molecules [29,30], our procedure may be combined with the techniques of molecular alignment and orientation to reveal the structure effect on the PQNDs of high-lying Rydberg states of molecules or molecular fragments.

ACKNOWLEDGMENTS

We thank Prof. J. Chen and Prof. X. L. Hao for many stimulating discussions. We thank Y. Q. Xu, H. Y. Sun, C. Z. Wan, Y. Wang, and Q. F. Chen for technical support of the laser system, electronic devices, and vacuum system. This work is supported by the National Key Research and Development Program (Grant No. 2019YFA0307702), the National Natural Science Foundation of China (Grants No. 11774387, No. 11874392, No. 11834015, No. 11974383, No. 11674356, No. 11922413, and No. 11527807), the Strategic Priority Re-

search Program of the Chinese Academy of Sciences (Grant No. XDB21010400), the Science and Technology Department

of Hubei Province (Grant No. 2019CFA035) and the K. C. Wong Education Foundation.

- [1] G. G. Paulus, W. Nicklich, H. Xu, P. Lambropoulos, and H. Walther, *Phys. Rev. Lett.* **72**, 2851 (1994).
- [2] W. Becker, X. J. Liu, P. J. Ho, and J. H. Eberly, *Rev. Mod. Phys.* **84**, 1011 (2012).
- [3] A. D. Shiner, B. E. Schmidt, C. Trallero-Herrero, H. J. Wörner, S. Patchkovskii, P. B. Corkum, J. C. Kieffer, F. Légaré, and D. M. Villeneuve, *Nat. Phys.* **7**, 464 (2011).
- [4] P. B. Corkum, *Phys. Rev. Lett.* **71**, 1994 (1993).
- [5] K. J. Schafer, B. Yang, L. F. DiMauro, and K. C. Kulander, *Phys. Rev. Lett.* **70**, 1599 (1993).
- [6] T. Nubbemeyer, K. Gorling, A. Saenz, U. Eichmann, and W. Sandner, *Phys. Rev. Lett.* **101**, 233001 (2008).
- [7] A. S. Landsman, A. N. Pfeiffer, C. Hofmann, M. Smolarski, C. Cirelli, and U. Keller, *New J. Phys.* **15**, 013001 (2013).
- [8] P. Ge and Y. Liu, *J. Phys. B* **50**, 125001 (2017).
- [9] K. Y. Huang, Q. Z. Xia, and L. B. Fu, *Phys. Rev. A* **87**, 033415 (2013).
- [10] Y. Zhao, Y. Zhou, J. Liang, Z. Zeng, Q. Ke, Y. Liu, M. Li, and P. Lu, *Opt. Express* **27**, 21689 (2019).
- [11] U. Eichmann, T. Nubbemeyer, H. Rottke, and W. Sandner, *Nature (London)* **461**, 1261 (2009).
- [12] Q. Z. Xia, L. B. Fu, and J. Liu, *Phys. Rev. A* **87**, 033404 (2013).
- [13] H. Zimmermann, J. Buller, S. Eilzer, and U. Eichmann, *Phys. Rev. Lett.* **114**, 123003 (2015).
- [14] N. I. Shvetsov-Shilovski, S. P. Goreslavski, S. V. Popruzhenko, and W. Becker, *Laser Phys.* **19**, 1550 (2009).
- [15] B. Manschwetus, T. Nubbemeyer, K. Gorling, G. Steinmeyer, U. Eichmann, H. Rottke, and W. Sandner, *Phys. Rev. Lett.* **102**, 113002 (2009).
- [16] T. Nubbemeyer, U. Eichmann, and W. Sandner, *J. Phys. B* **42**, 134010 (2009).
- [17] K. N. Shomsky, Z. S. Smith, and S. L. Haan, *Phys. Rev. A* **79**, 061402(R) (2009).
- [18] J. Wu, A. Vredenburg, B. Ulrich, L. Ph. H. Schmidt, M. Meckel, S. Voss, H. Sann, H. Kim, T. Jahnke, and R. Dörner, *Phys. Rev. Lett.* **107**, 043003 (2011).
- [19] H. Zimmermann, S. Patchkovskii, M. Ivanov, and U. Eichmann, *Phys. Rev. Lett.* **118**, 013003 (2017).
- [20] D. Chetty, R. D. Glover, B. A. deHarak, X. M. Tong, H. Xu, T. Pauly, N. Smith, K. R. Hamilton, K. Bartschat, J. P. Ziegler, N. Douguet, A. N. Luiten, P. S. Light, I. V. Litvinyuk, and R. T. Sang, *Phys. Rev. A* **101**, 053402 (2020).
- [21] H. Lv, W. Zuo, L. Zhao, H. Xu, M. Jin, D. Ding, S. Hu, and J. Chen, *Phys. Rev. A* **93**, 033415 (2016).
- [22] B. Piraux, F. Mota-Furtado, P. F. O'Mahony, A. Galstyan, and Yu V. Popov, *Phys. Rev. A* **96**, 043403 (2017).
- [23] Q. Li, X. M. Tong, T. Morishita, H. Wei, and C. D. Lin, *Phys. Rev. A* **89**, 023421 (2014).
- [24] S. Hu, X. Hao, H. Lv, M. Liu, T. Yang, H. Xu, M. Jin, D. Ding, Q. Li, W. Li, W. Becker, and J. Chen, *Opt. Express* **27**, 31629 (2019).
- [25] S. P. Xu, M. Q. Liu, S. L. Hu, Z. Shu, W. Quan, Z. L. Xiao, Y. Zhou, M. Z. Wei, M. Zhao, R. P. Sun, Y. L. Wang, L. Q. Hua, C. Gong, X. Y. Lai, J. Chen, and X. J. Liu, *Phys. Rev. A* **102**, 043104 (2020).
- [26] S. Larimian, S. Erattupuzha, C. Lemell, S. Yoshida, S. Nagele, R. Maurer, A. Baltuška, J. Burgdorfer, M. Kitzler, and X. Xie, *Phys. Rev. A* **94**, 033401 (2016).
- [27] S. Larimian, C. Lemell, V. Stummer, J. W. Geng, S. Roither, D. Kartashov, L. Zhang, M. X. Wang, Q. Gong, L. Y. Peng, S. Yoshida, J. Burgdorfer, A. Baltuška, M. Kitzler, and X. Xie, *Phys. Rev. A* **96**, 021403(R) (2017).
- [28] S. Larimian, S. Erattupuzha, A. Baltuška, M. Kitzler-Zeiler, and X. Xie, *Phys. Rev. Research* **2**, 013021 (2020).
- [29] W. Zhang, Z. Yu, X. Gong, J. Wang, P. Lu, H. Li, Q. Song, Q. Ji, K. Lin, J. Ma, H. Li, F. Sun, J. Qiang, H. Zeng, F. He, and J. Wu, *Phys. Rev. Lett.* **119**, 253202 (2017).
- [30] W. Zhang, P. Lu, X. Gong, H. Li, Q. Ji, K. Lin, J. Ma, H. Li, F. Sun, J. Qiang, F. Chen, J. Tong, and J. Wu, *Phys. Rev. A* **101**, 033401 (2020).
- [31] J. Ullrich, R. Moshhammer, A. Dorn, R. Döner, L. Ph. H. Schmidt, and H. Schmidt-Böcking, *Rep. Prog. Phys.* **66**, 1463 (2003).
- [32] T. Jahnke, Th. Weber, T. Osipov, A. L. Landers, O. Jagutzki, L. Ph. H. Schmidt, C. L. Cocke, M. H. Prior, H. Schmidt-Böcking, and R. Dörner, *J. Electron. Spectrosc. Relat. Phenom.* **141**, 229 (2004).
- [33] Y. Chen, S. Yu, R. Sun, C. Gong, L. Hua, X. Lai, W. Quan, and X. Liu, *Chin. Phys. Lett.* **33**, 043301 (2016).
- [34] M. Z. Wei, W. Quan, R. P. Sun, S. P. Xu, Z. L. Xiao, Y. Zhou, M. Zhao, X. L. Hao, C. X. Duan, and X. J. Liu, *Phys. Rev. A* **98**, 063418 (2018).
- [35] W. Quan, V. V. Serov, M. Z. Wei, M. Zhao, Y. Zhou, Y. L. Wang, X. Y. Lai, A. S. Kheifets, and X. J. Liu, *Phys. Rev. Lett.* **123**, 223204 (2019).
- [36] R. P. Sun, X. Y. Lai, S. G. Yu, Y. L. Wang, S. P. Xu, W. Quan, and X. J. Liu, *Phys. Rev. Lett.* **122**, 193202 (2019).
- [37] R. J. Damburg and V. V. Kolosov, *J. Phys. B* **12**, 2637 (1979).
- [38] R. J. Damburg and V. V. Kolosov, *J. Phys. B* **11**, 1921 (1978).
- [39] S. P. Alliluev and I. A. Malkin, *Sov. Phys. JETP* **39**, 627 (1974).
- [40] A. Müller, D. S. Belić, B. D. DePaola, N. Djurić, G. H. Dunn, D. W. Mueller, and C. Timmer, *Phys. Rev. A* **36**, 599 (1987).
- [41] W. Quan, X. Hao, Y. Chen, S. Yu, S. Xu, Y. Wang, R. Sun, X. Lai, C. Wu, Q. Gong, X. He, X. Liu, and J. Chen, *Sci. Rep.* **6**, 27108 (2016).
- [42] J. Chen, J. Liu, and S. G. Chen, *Phys. Rev. A* **61**, 033402 (2000).
- [43] X. L. Hao, G. Q. Wang, X. Y. Jia, W. D. Li, J. Liu, and J. Chen, *Phys. Rev. A* **80**, 023408 (2009).
- [44] W. Quan, Z. Lin, M. Wu, H. Kang, H. Liu, X. Liu, J. Chen, J. Liu, X. T. He, S. G. Chen, H. Xiong, L. Guo, H. Xu, Y. Fu, Y. Cheng, and Z. Z. Xu, *Phys. Rev. Lett.* **103**, 093001 (2009).
- [45] Y. L. Wang, S. P. Xu, Y. J. Chen, H. P. Kang, X. Y. Lai, W. Quan, X. J. Liu, X. L. Hao, W. D. Li, S. L. Hu, J. Chen, W. Becker, W.

- Chu, J. Yao, B. Zeng, Y. Cheng, and Z. Z. Xu, *Phys. Rev. A* **95**, 063415 (2017).
- [46] M. V. Ammosov, N. B. Delone, and V. P. Krainov, *Sov. Phys. JETP* **64**, 1191 (1986).
- [47] N. B. Delone and V. P. Krainov, *J. Opt. Soc. Am. B* **8**, 1207 (1991).
- [48] B. Hu, J. Liu, and S.-G. Chen, *Phys. Lett. A* **236**, 533 (1997).
- [49] T. Brabec, M. Y. Ivanov, and P. B. Corkum, *Phys. Rev. A* **54**, R2551 (1996).
- [50] J. Chen, J. Liu, L. B. Fu, and W. M. Zheng, *Phys. Rev. A* **63**, 011404(R) (2000).
- [51] L. B. Fu, J. Liu, J. Chen, and S. G. Chen, *Phys. Rev. A* **63**, 043416 (2001).
- [52] J. Chen, J. Liu, and W. M. Zheng, *Phys. Rev. A* **66**, 043410 (2002).
- [53] D. F. Ye, X. Liu, and J. Liu, *Phys. Rev. Lett.* **101**, 233003 (2008).
- [54] Q. Z. Xia, D. F. Ye, L. B. Fu, X. Y. Han, and J. Liu, *Sci. Rep.* **5**, 11473 (2015).
- [55] H. Suno, L. Andric, T. P. Grozdanov, and R. McCarroll, *Phys. Rev. A* **59**, 524 (1999).
- [56] A. M. Alonso, L. Gurung, B. A. D. Sukra, S. D. Hogan, and D. B. Cassidy, *Phys. Rev. A* **98**, 053417 (2018).
- [57] B. Shan, S. Ghimire, and Z. Chang, *J. Mod. Opt.* **52**, 277 (2005).
- [58] D. B. Milošević, W. Becker, and R. Kopold, *Phys. Rev. A* **61**, 063403 (2000).